# Stress effects on the Raman spectrum of an amorphous material: Theory and experiment on a-Si:H

David A. Strubbe, Eric C. Johlin, Timothy R. Kirkpatrick, Tonio Buonassisi, and Jeffrey C. Grossman

Phys. Rev. B **92**, 241202 — Published 18 December 2015

DOI: 10.1103/PhysRevB.92.241202

# Stress effects on the Raman spectrum of an amorphous material: theory and experiment on a-Si:H

David A. Strubbe,[1, a] Eric C. Johlin,[1, 2, b] Timothy R. Kirkpatrick,[2] Tonio Buonassisi,[2] and Jeffrey C. Grossman[1, c]

[1]*Department of Materials Science and Engineering, Massachusetts Institute of Technology, Cambridge, MA 02139*

[2]*Department of Mechanical Engineering, Massachusetts Institute of Technology, Cambridge, MA 02139*

## Abstract

Strain in a material induces shifts in vibrational frequencies, which is a probe of the nature of the vibrations and interatomic potentials, and can be used to map local stress/strain distributions via Raman microscopy. This method is standard for crystalline silicon devices, but due to lack of calibration relations, it has not been applied to amorphous materials such as hydrogenated amorphous silicon (a-Si:H), a widely studied material for thin-film photovoltaic and electronic devices. We calculated the Raman spectrum of a-Si:H *ab initio* under different strains $\epsilon$ and found peak shifts $\Delta\omega = \left(-460 \pm 10 \text{ cm}^{-1}\right) \text{Tr } \epsilon$. This proportionality to the trace of the strain is the general form for isotropic amorphous vibrational modes, as we show by symmetry analysis and explicit computation. We also performed Raman measurements under strain and found a consistent coefficient of $-510 \pm 120$ cm$^{-1}$. These results demonstrate that a reliable calibration for the Raman/strain relation can be achieved even for the broad peaks of an amorphous material, with similar accuracy and precision as for crystalline materials.

Hydrogenated amorphous silicon (a-Si:H) is a photovoltaic material which has been studied for decades and used commercially.[1,2] Compared to the more commonly used crystalline Si (c-Si), a-Si:H has advantages in stronger visible absorption, cheaper and faster fabrication, and the potential for flexible thin-film devices.[2] a-Si:H can be used alone or in heterojunction cells where it can passivate the surface of c-Si active layers.[2,3] It also has applications for solar water-splitting,[4] thin-film transistors,[5] bolometers,[6] particle detectors,[7] and microelectromechanical systems.[8] However, widespread adoption has been limited by two important disadvantages: mobilities degrade under illumination via the Staebler-Wronski effect,[9] and efficiencies are significantly limited by low hole mobility.[10]

Crystallization to c-Si is used to create higher-mobility microcrystalline Si ($\mu$c-Si),[11,12] and could circumvent low hole mobility in a-Si:H by adding nanostructured charge-extraction channels.[13] Conversion to denser c-Si induces stress, as does deposition,[14] thermal expansion, or other processing. Stress is often large in thin films (and may be inhomogeneous[15]), and is a critical parameter in a-Si:H as it affects mobilities,[5] defects,[16] the Staebler-Wronski effect,[17] and mechanical failure properties,[18] and potentially transport via band-bending.[19]

A standard technique to understand stress effects on c-Si microelectronic devices is Raman microscopy,[20,21] which yields a spatial distribution of stress in the device (unlike X-ray diffraction measurements[22]). The Raman-active optical phonon modes in c-Si are shifted to higher frequency by compressive strain (and *vice versa*), with established coefficients[23,24] which are used to translate peak positions to local strain. Raman microscopy is also commonly used for a-Si:H and $\mu$c-Si, generally for mapping the quality or crystallinity of films via the position and width of the transverse optical (TO) peak[11] (analogous to the optical phonons of c-Si). In contrast to the case for c-Si, for a-Si:H the relation between peak positions and strain has not been clear, preventing detailed understanding of stress; with accurate knowledge of the coefficient, these studies would be able to map stress too. This property also serves as a probe of vibrations and interatomic potentials.[24,25] Stress effects on Raman peaks (also called "piezo-Raman" or "phonon deformation potentials") have been studied for various crystalline semiconductors.[26] However there has been little work on amorphous materials, confined to experimental reports on carbon[27] or carbon and SiC fibers,[28] without theory or consideration of dependence on strain pattern.

In previous work, Fabian and Allen[25] calculated the effect of hydrostatic pressure on the vibrational modes of large supercells of a-Si (non-hydrogenated) via Stillinger-Weber

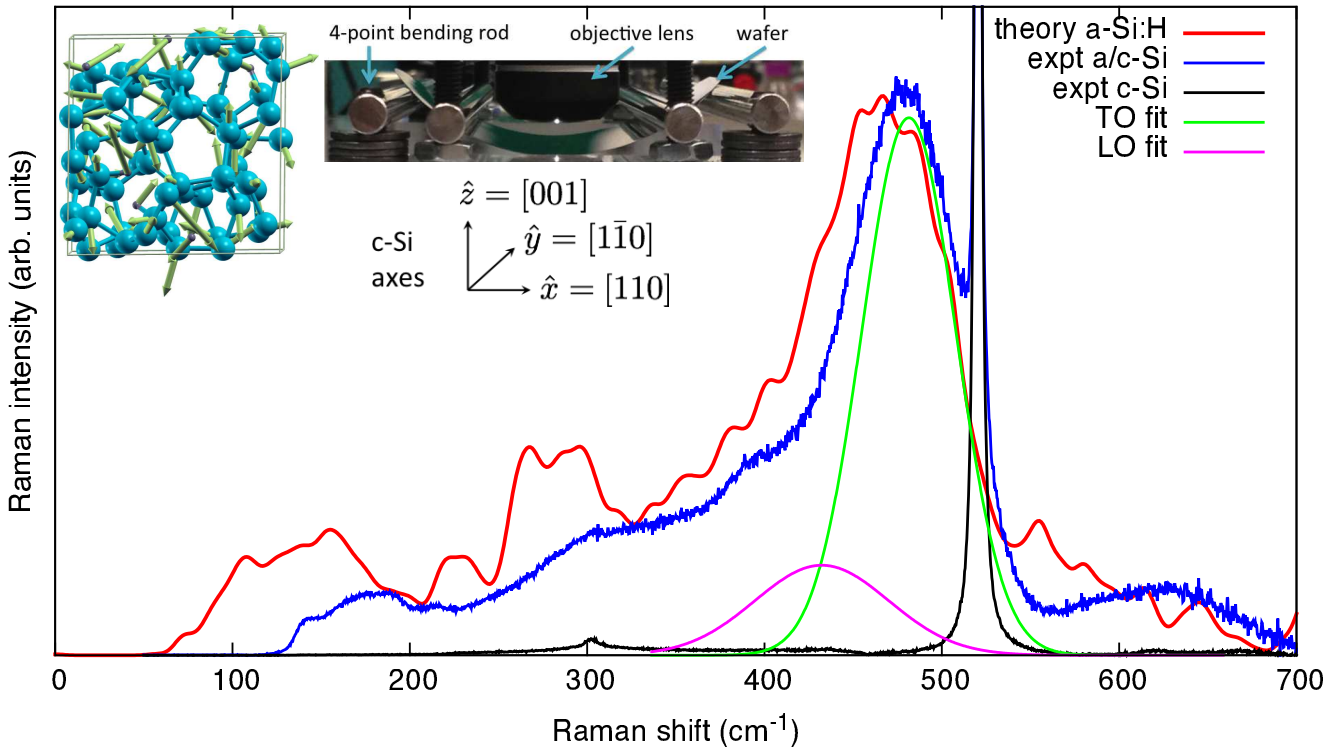


FIG. 1: Theoretically calculated Raman spectrum for a-Si:H, and measured Raman spectra for a-Si:H on c-Si, and c-Si, reduced by removal of the temperature- and frequency-dependent factors (see text), with fits to a-Si:H transverse and longitudinal optical peaks (TO, LO) in measured spectrum. Left inset: Example calculated $Si_{64}H_6$ TO vibrational mode. Right inset: Experimental setup for Raman microscopy with four-point bending, and orientation of crystal axes in c-Si wafer.

classical potentials, but did not compute Raman spectra. An *ab initio* study[29] calculated vibrational modes (but not stress effects) by density-functional theory, but obtained Raman spectra only via semi-empirical bond polarizability models, which gave a significant discrepancy from experiment.

Experimental work by Ishidate *et al.*[30] and Hishikawa[31] studied the effect of pressure and bending on the Raman spectrum of a-Si:H. However, it is not clear how to extract a strain coefficient (the general materials property) from these works, due to insufficient detail about the experimental setups and stress applied.[32] Therefore only qualitative interpretations of a-Si:H stress from Raman spectroscopy have been possible.[12,33]

In this Rapid Communication, we present a fully *ab initio* computation of the Raman spectrum of a-Si:H under neutral and applied strain, complemented with a systematic experimental study. We show the general form of peak shifts with strain in an amorphous

material, and obtain close agreement between theory and experiment in the spectra and the strain coefficient for the TO peak shift. This provides the calibration needed for quantitative strain mapping of a-Si:H films for optical, electronic, and mechanical devices, with sufficient sensitivity for applications of interest (analyzed in SI[34]).

Our theoretical calculations use an ensemble of periodic structures generated by the standard classical Monte Carlo Wooten-Winer-Weaire approach,[35] representing local regions which are averaged to find the overall properties of a-Si:H. We add hydrogen to the sample by breaking randomly chosen Si-Si bonds at the beginning of the process, as in our previous work[36] and implemented in our CHASSM code.[37,38] We use 34 structures to obtain a smooth Raman spectrum, each with formula $Si_{64}H_6$ to emulate a typical 10% hydrogen content, in a cube roughly 11 Å on a side. Density-functional theory (DFT) and density-functional perturbation theory (DFPT)[39] calculations were performed with the Quantum ESPRESSO code (version 5.1)[40] and the local-density approximation,[41] to obtain the phonons at $\mathbf{q} = \Gamma$ and their first-order Raman intensities.[42] These widely used calculation methods have been found to be generally reliable for vibrational properties.[39] Each structure was calculated also with 0.5% uniaxial compressive and tensile strain, which gave a resolvable effect within a linear regime. We study the unpolarized (isotropically averaged) Raman spectrum, with a Gaussian broadening of 5 $cm^{-1}$ standard deviation, comparable to the separation between vibrational modes in an individual structure.

We benchmark the accuracy of our theoretical approach for strain effects on the Raman spectrum by calculations on c-Si under [100] uniaxial strain. The Raman-active zone-center optical phonons have a frequency of 514 $cm^{-1}$, a typical DFT level of agreement with the experimental value of 520 $cm^{-1}$.[43] The slopes of the split modes are in reasonable agreement with the measured values for bulk c-Si,[24] though slightly too small: singly-degenerate, calculated $-424$ $cm^{-1}$ *vs.* measured $p/2\omega_0^c = -481 \pm 20$ $cm^{-1}$; doubly-degenerate, calculated $-547$ $cm^{-1}$ *vs.* measured $q/2\omega_0^c = -601 \pm 20$ $cm^{-1}$.

For the experimental measurements, intrinsic a-Si:H films were deposited using a plasma-enhanced chemical vapor deposition tool (PECVD, Surface Technology Systems) to a thickness of $\sim 1.1$ $\mu$m, on 3 inch diameter 100 $\mu$m ($\pm$ 15 $\mu$m) thick <100> c-Si wafers. Raman microscopy was performed using a Horiba LabRam-HR800 Raman spectrometer with a 632.8 nm excitation beam focused to a 1 $\mu$m spot size. Compressive stress was applied to the a-Si:H film by bending the wafer in a custom-built four-point bending apparatus, as shown in

the inset of Fig. 1.

The obtained Raman spectra are shown in Fig. 1. The experimental results have been "reduced" by multiplication by the factor $\omega\left(1-e^{-\hbar\omega/kT}\right)$ (where $\omega$ is the Raman shift and $T = 300$ K is the temperature), which is the basis for Raman temperature determination.[44] We can then directly compare to the calculated absolute Raman intensities,[42,45] in arbitrary units since we do not have an experimental intensity calibration. The peaks in a-Si:H are conventionally named by the corresponding peaks in the vibrational density of states of c-Si.[45,46] The position of the transverse optical (TO) peak, the focus of this work, is at 470 $cm^{-1}$ (theory) and 480 $cm^{-1}$ (experiment), which agrees well within the typical errors of DFT and the variation among a-Si:H samples.[31] An example calculated vibrational mode in the TO peak is shown in the inset of Fig. 1. The longitudinal optical (LO) shoulder near 400 $cm^{-1}$ is also in good agreement. The low-energy spectrum agrees less well due to the more delocalized modes[25] and sensitivity to the size of the calculated supercells. The strong peak at 520 $cm^{-1}$ in the experiment is due to the underlying c-Si substrate, which also has a small peak at 300 $cm^{-1}$ due to second-order Raman scattering.[47] After a linear baseline correction, the experimental Raman spectra were fit to a sum of 3 Gaussians for the a-Si:H features[30] and a Lorentzian for c-Si[47] according to standard practice; LO and TO fits shown in Fig. 1 and SI.[34] We underscore the significant improvement in theoretical agreement with experiment, compared to the previous DFT/semi-empirical Raman work[29] which underestimated the TO peak by 50 $cm^{-1}$ and did not show the other peaks. We can now quantitatively predict the strain effects on the spectrum.

We now focus on the region $400-550$ $cm^{-1}$ around the a-Si:H TO peak and c-Si optical modes, and add the calculated spectra under 0.5% compressive and tensile uniaxial strains, and the measured spectrum under 0.33% compressive uniaxial strain, as shown in Fig. 2. The shifts to lower energies under tensile strain and higher energies under compressive strain can be seen in theory and experiment, for both the a-Si:H and c-Si peaks.

To analyze the strain effect in a-Si:H in our calculation, we make a one-to-one correspondence between the discrete vibrational modes in a supercell structure at each strain level. We find the Raman intensity change with strain is a small and almost uniform scaling over the spectrum. As a result, the strain effect on peak positions can be described by considering just the vibrational frequencies. The $\pm 0.5\%$ strain was confirmed to be in the linear regime by plotting frequencies over a range of strains.

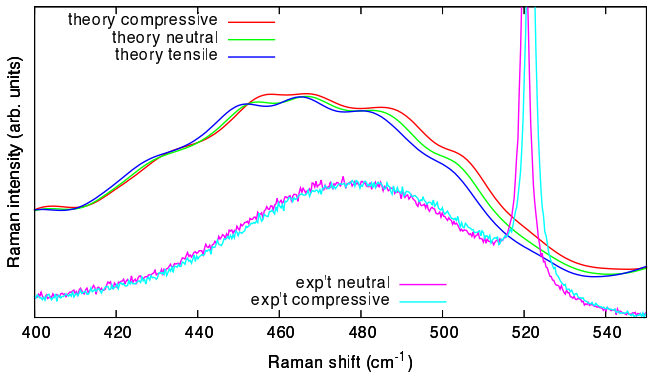


FIG. 2: Effect of strain on the Raman spectra: theoretical calculations on a-Si:H with neutral strain and 0.5% compressive and tensile strains, and a-Si:H on c-Si with neutral strain and 0.33% compressive strain, with peaks blue-shifted by compressive strain and *vice versa*.

For each mode in each structure, we compute the derivatives of the frequency in the compressive and tensile strain directions. These derivatives are closely related to the mode Grüneisen parameters $\gamma = -\frac{1}{\omega}\frac{d\omega}{d\epsilon}$, and are shown in full in SI.[34] We perform an average (weighted by the Raman intensities) over the derivatives of modes with frequencies 450 – 490 $\mathrm{cm}^{-1}$, yielding an overall TO peak position derivative of $460 \pm 10$ $\mathrm{cm}^{-1}$. The uncertainty is taken as the standard error of the mean, taking only the different structures as independent.

It is difficult to determine the strain sufficiently accurately from our wafer curvature via Stoney's equation,[48] and this would give only an averaged strain over the wafer. Instead we use the c-Si Raman shifts as an internal calibration of the local strain at the beam spot. We exploit the fact that our Raman measurements show both the a-Si:H thin film and the top of the underlying c-Si substrate (Fig. 1), given the penetration depth of 1 $\mu$m for a-Si:H and c-Si.[2]

To perform the calibration, we relate the c-Si peak shift to uniaxial strain according to the approach of Refs. 49 and 20. The geometry of our four-point bending setup (inset in Fig. 1), results in uniaxial stress in [110] ($x$) in the roughly rectangular region between the rods, according to the usual plane stress assumptions.[50] The optical mode detected in our backscattering geometry is shifted from the unstrained frequency $\omega_0^c = 520$ $\mathrm{cm}^{-1}$ (Ref. 43) proportionally to the strain $\epsilon_{xx}$ as $\Delta\omega^c = b\epsilon_{xx}$, where

$$b = \left[-p\nu_{xz}^c + q\left(1-\nu_{xy}^c\right)\right]/2\omega_0^c = -330 \pm 70 \text{ cm}^{-1} \quad (1)$$

(more detail in SI[34]). We use c-Si Poisson ratios $\nu_{xy}^c = 0.064$ and $\nu_{xz}^c = 0.28$,[51] and the

strain coefficients $p = -1.25 \pm 0.25\ (\omega_0^c)^2$ and $q = -1.87\ \pm 0.37\,(\omega_0^c)^2$ from an experiment with the same 632.8 nm excitation as in this work.[23] Due to stress relaxation (*i.e.* greater Poisson ratio $\nu_{zx}^c$) near the surface), these strain coefficients are lower than those obtained at 1064 nm,[24] with a signal penetrating about 100 $\mu$m into the bulk.[2]

Next we connect the strain in c-Si to the strain in the a-Si:H film, specifically the trace Tr $\epsilon^a$ (justified below). Assuming no slip from the substrate, the strain $\epsilon_{xx}$ is the same in the a-Si:H film. Taking into account the other directions,

$$\text{Tr}\ \epsilon^a = d\epsilon_{xx} = \left(1 - \nu_{xy}^c - \nu^a\right)\epsilon_{xx}, \tag{2}$$

where the coefficient $d = 0.69 \pm 0.05$, using $\nu^a = 0.25 \pm 0.05$ for dense films of 10% H.[52]

We now infer strain for each position of the four-point bending setup from the c-Si peak shift as Tr $\epsilon^a = d\Delta\omega^c/b$. Given a Young's modulus around 80 GPa[53] and strain 0.33%, maximum stress was 260 MPa, well within the range from PECVD growth.[14] We plot the experimental a-Si:H peak position with respect to strain in Fig. 3, showing a linear relationship with regression slope $-510 \pm 120$ cm$^{-1}$; the uncertainty is mostly from the c-Si calibration values and $\nu^a$. The plotted line with the theoretical slope (and experimental intercept) also fits the data well. Note that if uniaxial strain rather than stress had been assumed in the wafer, we would have obtained $b = q/2\omega_0^c$ and $d = 1$, yielding almost the same value $s = -520 \pm 110$ cm$^{-1}$, showing insensitivity to the exact mechanical boundary conditions. We quote our result with respect to strain, rather than stress, to be more general since the shifts are due directly to bond length changes, and the Young's modulus relating stress and strain can vary by a factor of 2 depending on synthesis conditions.[53]

Finally, we demonstrate the general form of the a-Si:H TO peak shift with strain. c-Si has a complicated dependence on the strain pattern due to its symmetry, but a-Si:H is isotropic except at very short length scales. For example, in our 70-atom cells, the calculated dielectric constant is $\sim 15$ with anisotropy only $\sim 0.6$. Due to this effective symmetry, the calculated vibrational modes in the TO peak are delocalized, roughly isotropic, and sensitive to Raman scattering in any polarization (see inset of Fig. 1). Nonetheless, without any true symmetry, there is no counterpart to the three-fold degeneracy of the c-Si optical phonons. As a result, the TO band transforms as a scalar rather than a vector as for c-Si. Since there is no degeneracy there is no splitting as of the c-Si modes.[23] In general, the frequency shift for such a scalar mode in a material would be $\Delta\omega = \sum_{ij} S_{ij}\epsilon_{ij}$ where $S$, like $\epsilon$, is a

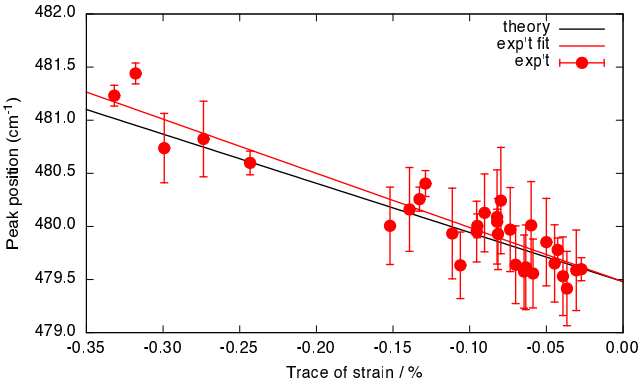


FIG. 3: Shifts in a-Si:H Raman peak positions *vs.* strain from uniaxial stress, inferred from c-Si peak shifts. Slopes: $-460 \pm 10$ cm$^{-1}$ (theory), $-510 \pm 120$ cm$^{-1}$ (exp't fit). Both lines use experimental intercept. Relation can be used to infer local strain from Raman microscopy.

| | DFT | model | exp't | classical[25] |
|---|---|---|---|---|
| $\omega_c$ / cm$^{-1}$ | 514 | | 520[43] | 605 |
| $\omega_a$ / cm$^{-1}$ | 470 | 430[29] | 480 | 525 |
| $\gamma_c$ | 0.98 | | 1.08[24] | 0.8 |
| $\gamma_a$ | 0.98 | | 1.06 | 1.0 |

TABLE I: Raman transverse optical (TO) peak positions $\omega$ and mode Grüneisen parameters $\gamma$ for crystalline (c) and amorphous (a) Si, from: DFT, DFT plus bond polarizability model, experiment, and classical potentials. From this work unless cited.

symmetric rank-2 tensor. For an isotropic material, symmetry dictates $S_{ij} = s\delta_{ij}$. Therefore the peak shift is determined only by the trace of the strain tensor:

$$\Delta\omega^a = s\left(\epsilon^a_{xx} + \epsilon^a_{yy} + \epsilon^a_{zz}\right) = s \text{ Tr } \epsilon^a. \tag{3}$$

Indeed, we find in our calculations that the Raman spectrum is almost indistinguishable for applied uniaxial, biaxial, or triaxial strain tensors with the same trace, even on a single 70-atom cell (see SI[34]). This analysis applies generally to isotropic amorphous vibrational modes.

We find that our theoretical ($-460\pm10$ cm$^{-1}$) and experimental ($-510\pm120$ cm$^{-1}$) values are consistent, supporting the accuracy of the results. The agreement also implies lack of slip between the a-Si:H film and c-Si substrate, as has been argued for thermal expansion

of epitaxial graphene,[54] as slip would relax strain and lower the measured coefficient. The value is similar to the isotropic one for c-Si (surface), $-430 \pm 90$ cm$^{-1}$.[23]

In Table I we compare theoretical and experiment results for peak frequencies and mode Grüneisen parameters $\gamma$ of c-Si and a-Si:H. $\gamma$, describing anharmonicity, is important in the theory of thermal expansion and phonon transport.[55] The importance of *ab initio* calculations is shown by the much improved agreement with experimental $\omega$ and $\gamma$, compared to classical potentials.[25]

To conclude, we obtained the Raman spectra of a-Si:H from first principles in good agreement with experiment. We computed the strain coefficient for the TO peak from theory as $-460 \pm 10$ cm$^{-1}$, and measured a consistent value of $-510 \pm 120$ cm$^{-1}$, achieving an experimental uncertainty similar to that for c-Si surfaces despite having to deconvolve much broader peaks. We demonstrated, by symmetry analysis and explicit computation, the general form of strain effects on isotropic amorphous vibrational mode frequencies, as $\Delta\omega = s$ Tr $\epsilon$, determined only by the trace of the strain. The actual strain pattern (as in c-Si) needs to be provided by elasticity modeling.[20] Our results provide consistent and reliable calibration for the Raman/strain relation, enabling micro-Raman mapping of strain in a-Si:H films for the further development of photovoltaic, electronic, and mechanical devices.

**Acknowledgments**

We acknowledge Nicola Ferralis and Nouar Tabet for helpful discussions, and James Serdy for construction of the four-point bending setup. This work was supported by the Center for Clean Water and Energy at MIT and the King Fahd University of Petroleum and Minerals, Dhahran, Saudi Arabia under Project No. R1-CE-08. Computation was performed at the National Energy Research Scientific Computing Center at Lawrence Berkeley National Laboratory, a DOE Office of Science User Facility supported by the Office of Science of the U.S. Department of Energy under Contract No. DE-AC02-05CH11231. Fabrication was performed at the Center for Nanoscale Systems (CNS) at Harvard University, a member of the National Nanotechnology Infrastructure Network (NNIN), supported by the National

Science Foundation under NSF award no. ECS-0335765.

---

[a] Electronic address: dstrubbe@mit.edu

[b] Present address: FOM Institute AMOLF, 1098 XG Amsterdam, The Netherlands

[c] Electronic address: jcg@mit.edu

[1] J. Jean, P. R. Brown, R. L. Jaffe, T. Buonassisi, and V. Bulovic, Energy Environ. Sci. **8**, 1200 (2015).

[2] A. Shah, in *Solar Cells*, edited by T. Markvart, A. McEvoy, and L. Castañer (Elsevier, 2013), pp. 159 – 223, 2nd ed.

[3] B. M. George, J. Behrends, A. Schnegg, T. F. Schulze, M. Fehr, L. Korte, B. Rech, K. Lips, M. Rohrmüller, E. Rauls, et al., Phys. Rev. Lett. **110**, 136803 (2013).

[4] F. F. Abdi, L. Han, A. H. M. Smets, M. Zeman, B. Dam, and R. Van de Krol, Nat. Commun. **4**, 2195 (2013).

[5] H. Gleskova and S. Wagner, Appl. Phys. Lett. **79**, 3347 (2001).

[6] A. J. Syllaios, T. R. Schimert, R. W. Gooch, W. L. McCardel, B. A. Ritchey, and J. H. Tregilgas, MRS Proc. **609**, A14.4 (2000).

[7] A. Franco, Y. Riesen, M. Despeisse, N. Wyrsch, and C. Ballif, IEEE Trans. Nucl. Sci. **59**, 2614 (2012).

[8] S. Chang and S. Sivoththaman, J. Micromech. Microeng. **16**, 1307 (2006).

[9] D. L. Staebler and C. R. Wronski, Appl. Phys. Lett. **31**, 292 (1977).

[10] J. Mattheis, J. H. Werner, and U. Rau, Phys. Rev. B **77**, 085203 (2008).

[11] A. H. Mahan, M. S. Dabney, D. Molina Piper, and W. Nemeth, J. Appl. Phys. **115**, 083502 (2014).

[12] K. Wu, X. Q. Yan, and M. W. Chen, Appl. Phys. Lett. **91**, 101903 (2007).

[13] N. Tabet, A. Al-Sayoud, S. Said, X. Yang, Y. Yang, A. Syed, E. Diallo, Z. Wang, X. Wang, E. Johlin, et al., in *38th IEEE Photovoltaic Specialists Conference* (2012), pp. 000364–000366.

[14] E. Johlin, N. Tabet, S. Castro-Galnares, A. Abdallah, M. I. Bertoni, T. Asafa, J. C. Grossman, S. Said, and T. Buonassisi, Phys. Rev. B **85**, 075202 (2012).

[15] V. Paillard, P. Puech, R. Sirvin, S. Hamma, and P. Roca i Cabarrocas, J. Appl. Phys. **90**, 3276 (2001).

[16] E. Johlin, C. B. Simmons, T. Buonassisi, and J. C. Grossman, Phys. Rev. B **90**, 104103 (2014).

[17] M. Stutzmann, Appl. Phys. Lett. **47**, 21 (1985).

[18] J. Pomeroy, P. Gkotsis, M. Zhu, G. Leighton, P. Kirby, and M. Kuball, J. Microelectromech. Syst. **17**, 1315 (2008).

[19] J. Feng, X. Qian, C.-W. Huang, and J. Li, Nat. Photon. **6**, 866 (2012).

[20] I. De Wolf, Semicond. Sci. Technol. **11**, 139 (1996).

[21] E. Bonera, M. Fanciulli, and D. N. Batchelder, J. Appl. Phys. **94**, 2729 (2003).

[22] X. L. Wu, S. Tong, X. N. Liu, X. M. Bao, S. S. Jiang, D. Feng, and G. G. Siu, Appl. Phys. Lett. **70**, 838 (1997).

[23] E. Anastassakis, A. Pinczuk, E. Burstein, F. Pollak, and M. Cardona, Solid State Commun. **8**, 133 (1970).

[24] E. Anastassakis, A. Cantarero, and M. Cardona, Phys. Rev. B **41**, 7529 (1990).

[25] J. Fabian and P. B. Allen, Phys. Rev. Lett. **79**, 1885 (1997).

[26] E. Anastassakis, in *Light Scattering in Semiconductor Structures and Superlattices*, edited by D. J. Lockwood and J. F. Young (Springer US, 1991), vol. 273 of *NATO ASI Series*, pp. 173–196.

[27] J.-K. Shin, C. S. Lee, K.-R. Lee, and K. Y. Eun, Appl. Phys. Lett. **78**, 631 (2001).

[28] G. Gouadec and P. Colomban, Prog. Cryst. Growth Charact. Mater. **53**, 1 (2007).

[29] R. M. Ribeiro, V. J. B. Torres, M. I. Vasilevskiy, A. Barros, and P. R. Briddon, phys. stat. sol. (c) **7**, 1432 (2010).

[30] T. Ishidate, K. Inoue, K. Tsuji, and S. Minomura, Solid State Commun. **42**, 197 (1982).

[31] Y. Hishikawa, J. Appl. Phys. **62**, 3150 (1987).

[32] Y. Hishikawa, private communication (2015).

[33] A. Vetushka, M. Ledinský, J. Stuchlík, T. Mates, A. Fejfar, and J. Kočka, J. Non-Cryst. Solids **354**, 2235 (2008).

[34] See Supplemental Material at [URL will be inserted by publisher] for more details on theoretical calculations, experimental methods, strain modeling, and strain mapping.

[35] F. Wooten, K. Winer, and D. Weaire, Phys. Rev. Lett. **54**, 1392 (1985).

[36] E. Johlin, L. K. Wagner, T. Buonassisi, and J. C. Grossman, Phys. Rev. Lett. **110**, 146805 (2013).

[37] L. K. Wagner and J. C. Grossman, Phys. Rev. Lett. **101**, 265501 (2008).

[38] D. A. Strubbe, L. K. Wagner, E. C. Johlin, and J. C. Grossman, in preparation (2015).

[39] S. Baroni, S. de Gironcoli, A. Dal Corso, and P. Giannozzi, Rev. Mod. Phys. **73**, 515 (2001).

[40] P. Giannozzi, S. Baroni, N. Bonini, M. Calandra, R. Car, C. Cavazzoni, D. Ceresoli, G. L. Chiarotti, M. Cococcioni, I. Dabo, et al., J. Phys.: Condens. Matter **21**, 395502 (2009).

[41] J. P. Perdew and A. Zunger, Phys. Rev. B **23**, 5048 (1981).

[42] M. Lazzeri and F. Mauri, Phys. Rev. Lett. **90**, 036401 (2003).

[43] J. H. Parker, D. W. Feldman, and M. Ashkin, Phys. Rev. **155**, 712 (1967).

[44] X. J. Gu, J. Raman Spectrosc. **27**, 83 (1996).

[45] J. E. Smith, M. H. Brodsky, B. L. Crowder, M. I. Nathan, and A. Pinczuk, Phys. Rev. Lett. **26**, 642 (1971).

[46] M. H. Brodsky, M. Cardona, and J. J. Cuomo, Phys. Rev. B **16**, 3556 (1977).

[47] P. A. Temple and C. E. Hathaway, Phys. Rev. B **7**, 3685 (1973).

[48] L. B. Freund and S. Suresh, *Thin Film Materials* (Cambridge University Press, 2003).

[49] S. Ganesan, A. Maradudin, and J. Oitmaa, Ann. Phys. **56**, 556 (1970).

[50] L. L. Bucciarelli Jr., *Engineering Mechanics of Solids: A First Course in Engineering* (2002), URL `http://web.mit.edu/emech/dontindex-build/full-text/emechbk_7.pdf`.

[51] M. Hopcroft, W. Nix, and T. Kenny, J. Microelectromech. Syst. **19**, 229 (2010).

[52] R. Kuschnereit, H. Fath, A. Kolomenskii, M. Szabadi, and P. Hess, Appl. Phys. A **61**, 269 (1995).

[53] X. Jiang, B. Goranchev, K. Schmidt, P. Grünberg, and K. Reichelt, J. Appl. Phys. **67**, 6772 (1990).

[54] N. Ferralis, R. Maboudian, and C. Carraro, Phys. Rev. B **83**, 081410 (2011).

[55] K. Esfarjani, G. Chen, and H. T. Stokes, Phys. Rev. B **84**, 085204 (2011).